Available online at www.sciencedirect.com
SCIENCE DIRECT®
Solar Energy 76 (2004) 475–484
SOLAR ENERGY
www.elsevier.com/locate/solener

Operational method for deriving high resolution direct normal irradiance from satellite data

C. Schillings [a,*], H. Mannstein [b], R. Meyer [b]

[a] *Deutsches Zentrum für Luft- und Raumfahrt, DLR-Stuttgart, Institut für Technische Thermodynamik, Pfaffenwaldring 38-40, D-70569 Stuttgart, Germany*

[b] *Deutsches Zentrum für Luft- und Raumfahrt, DLR-Oberpfaffenhofen, Institut für Physik der Atmosphäre, D-82234 Weßling, Germany*

Received 2 December 2002; received in revised form 27 May 2003; accepted 9 July 2003
Communicated by: Associate Editor Richard Perez

Abstract

Ground-based measurements of solar beam irradiance are expensive and rarely available especially in the sunbelt countries, the favourable regions for concentrating solar energy techniques. A method based on satellite data is presented that calculates hourly solar direct normal irradiance for large regions and for many years with high spatial resolution independently from ground measurements. The attenuation of solar irradiance due to scattering and absorption in the cloud-free atmosphere is calculated by a clear-sky broadband parameterisation model. It uses ozone optical depth from the Total Ozone Mapping Spectrometer, aerosol optical depth from the Global Aerosol Climatology Project and water vapour from the reanalysis of the National Centers for Environmental Prediction. Attenuation due to clouds is taken into account by a cloud index that is derived from the infrared and the visible channel of the geostationary Meteosat weather satellites. As clouds have the strongest impact on beam irradiance at ground, the resolution of the cloud parameterisation dominates the overall spatial and temporal resolution. The presented algorithm provides hourly data of direct normal irradiance related to the nominal 5×5 km^2 resolution of Meteosat.

1. Introduction

Planning and control of concentrating solar systems like parabolic troughs, heliostats or dish-stirling systems need information about the direct fraction of solar radiation. Contrary to the diffuse fraction, this beam irradiance can be focused in order to yield higher energy flux densities at the receiver. The direct normal irradiance (DNI) serves as reference for those systems. DNI is defined as the radiant flux density in the solar spectrum (0.3–3 μm) incident at the earth's surface perpendicular to the direction to the sun integrated over a small cone tracing the sun.

The demand for DNI-data will increase strongly as solar-thermal electrical power generation stands on the threshold of economic profitability. For all concentrating solar technologies knowledge of DNI at ground for each potential site is one of the most important parameters, because it strongly affects the performance of such systems. The areas of interest for solar-thermal power stations are located in the so-called sunbelt countries between latitudes around 10°–40° (North and South), where only few measurements of DNI are available today. Several hundreds of ground stations would be necessary to map the spatial variability of the solar irradiance for a larger region. This is practically impossible, because ground measurements suffer from high costs for purchasing of equipment, adequate maintenance and time-consuming data screening. In the available data we find many gaps due to failure of the sensors or the station itself. Sensor degradation or missing cleaning lead to errors. Satellite data can solve

* Corresponding author. Tel.: +49-0-711-6862-784; fax: +49-0-711-6862-783.
E-mail address: christoph.schillings@dlr.de (C. Schillings).

0038-092X/$ - see front matter © 2003 Elsevier Ltd. All rights reserved.
doi:10.1016/j.solener.2003.07.038

theses shortcomings. Data can be provided continuously in space and time. Missing or bad data are very rare. Also, satellite sensor degradation is well known and, thus, can be corrected for the whole data set using calibration data provided by EUMETSAT (2003). Another advantage is the availability of data for long periods backwards. An almost continuous data set is available since Meteosat-2, which was launched in June 1981.

Several solar radiation data with various spatial resolutions are available, e.g. the Surface Solar Energy data of NASA-SSE with low resolution (2.5°×2.5°, about 280 km×280 km) or the Climatological Solar Radiation data of NREL-CSR with medium resolution (40 km×40 km). High-precession ground measurements may be more accurate than satellite derived data for a specific site under consideration. But as Zelenka et al. (1999) show, only 25 km away from a ground station, hourly satellite-derived irradiance becomes more accurate than extrapolated ground measurements. That study was performed using global horizontal irradiance (GHI) measurements of several sites in Europe and north-east USA. For direct irradiance in arid zones this distance of 25 km could be less due to the higher variability of the DNI compared to GHI. On the other hand, the homogenous, usually cloud-free regions could lead to a further distance than 25 km. Furthermore, Meteosat measurements integrate spatially over at least 2.5×2.5 km^2. The integrated values may thus be more representative for a solar-thermal power station that covers approximately 1 km^2 for each installed 50 MW of power, than a single point measurement related to the same area.

Many approaches exist to derive the global irradiance at ground using geostationary satellite data. First studies were made in the late 1970s and in the 1980s (e.g. Tarpley, 1979; Möser and Raschke, 1983; Gautier et al., 1980; Pinker and Ewing, 1985; Cano et al., 1986). All of these methods relate the reflected sunlight measured by the Meteosat visible channel (VIS) covering the range 0.45–1.0 μm, to the global irradiance at the surface. The beam irradiance can be derived indirectly by estimating the diffuse component of solar radiation which is then subtracted from the global irradiance. (e.g. Stuhlmann et al., 1989; Hammer et al., 2003; Ineichen and Perez, 1999; Perez et al., 2002; Rigollier et al. (2001)). In case of DNI these methods are not as useful as for the derivation of global irradiance, as the sensitivity of the measurement in the VIS channel is poor with low sun angles (i.e. in the morning and late afternoon hours) while clouds can still be detected using the Meteosat infrared channel (IR), covering the range 10.5–12.5 μm. In addition, thin cirrus clouds, which can have a strong effect on the DNI, show up in the IR data, while their effect on VIS data and also on global irradiance is low. The most accurate methods to calculate irradiances are radiative transport models. State-of-the-art methods also take into account 3-D cloud effects using a Monte-Carlo model (Wyser et al., 2002; Mayer, 1999). These methods are very accurate for a known atmospheric state but need a long computing time, exact 3-D location and form of clouds and are therefore not recommendable to assess DNI for large areas. Processing almost 17,500 half-hourly Meteosat slots per year, computing time is a major factor to be handled. Therefore, cut backs in the accuracy are accepted. The presented method calculates hourly time series of the direct part of the solar broadband spectrum at ground for several years and for each pixel within the satellite image with respect to the Meteosat resolution in adequate computing time.

We use a global data-set of ozone, water vapour and aerosol optical thickness as the most important atmospheric constituents that attenuate the solar irradiance on its way through the cloud-free atmosphere. For cloudy conditions, infrared and visible data of the geostationary Meteosat-satellites are taken to get information on the effective cloud amount and effective cloud optical depth. With these data, DNI can be calculated independently from the availability of ground measurements. This paper gives a description of the used irradiance model, the used input parameters and the derivation of a cloud index from Meteosat data. A further paper by the same authors describes the application of the method for the Arabian peninsula and a validation of the calculated irradiances with ground measurements in Saudi Arabia.

2. Clear-sky parameterisation model

The calculation of solar direct normal irradiance at the ground is based on a clear-sky broadband parameterisation model developed by Bird and Hulstrom (1981) and modified by Iqbal (1983). Accuracy assessments and detailed comparisons with other parameterisation models in several studies (Gueymard, 1993; Battles et al., 2000) have shown that this model performs as one of the best for clear-sky conditions. Bird's clear-sky-model requires atmospheric input data on O_2, CO_2, ozone, water vapour and aerosol optical thickness (AOT) to calculate the broadband DNI_{clear} with

$$DNI_{clear} = E_0 \cdot \tau_R \cdot \tau_{gas} \cdot \tau_{ozone} \cdot \tau_{WV} \cdot \tau_{Ae} \quad (1)$$

with the transmission coefficients for the attenuation by Rayleigh-scattering τ_R, for the attenuation by absorption of equally distributed gases (mainly CO_2 and O_2) τ_{gas}, for the attenuation by absorption of atmospheric ozone τ_{ozone}, for the attenuation by absorption of water vapour τ_{WV} and for the attenuation by extinction of aerosols τ_{Ae}. The eccentricity corrected solar constant E_0 is derived by

$$E_0 = \bar{E}_0 \left(\frac{\bar{r}}{r}\right)^2 = \bar{E}_0 \left(1 + 0.033 \cos \frac{2\pi \times \text{doy}}{365}\right) \quad (2)$$

with the mean earth-sun distance $\bar{r}$, the actual earth-sun distance r, the day of year *doy* and the solar constant ($\bar{E}_0 = 1367$) W/m^2 according to Fröhlich and Brusa (1981)). Using this parameterisation model instead of an accurate radiative transfer model lead to a mean bias error of 2.9% and a root mean square error of 4.5% (Gueymard (1993). The functions to derive the transmission coefficients shown in Eq. (1) can be found in detail in Iqbal (1983). DNI_{clear} can be calculated for each point of time of the year if the actual air mass is known.

3. Atmospheric clear-sky parameters

The atmospheric constituents attenuate the incoming solar direct irradiance to a different extent. DNI is mostly influenced by clouds. Aerosol, water vapour, Rayleigh scattering, ozone, O_2 and CO_2, here called clear-sky parameters, also have a certain influence. Fig. 1 gives an example daily curve of the DNI at ground against the different atmospheric constituents, calculated by the method presented here. Although the clear-sky input parameters are kept constant during the day, their influence on the attenuation is stronger for higher zenith angles due to the longer path through the atmosphere. Without this effect the irradiance on a surface that is kept perpendicular to the incoming solar rays would be constant. As aerosols have the strongest influence on the direct irradiance at clear-sky conditions and are highly variable in space and time, data of this parameter should be as accurate as possible. To use most realistic data for the clear-sky parameters we try to apply the best available global observational data set which can easily be substituted if data with higher spatial and temporal resolution or higher accuracy become available.

The parameters Rayleigh scattering, ozone, water vapour and aerosol optical thickness described below are calculated taking into account the air mass-effect that is influenced by the solar zenith angle and the geographical elevation over sea level for the investigated site. Here the digital elevation model "global land one-km base elevation digital elevation model" (GLOBE) (Hastings and Dunbar, 1998) with a spatial horizontal resolution of 1 km^2 is used to correct altitude effects as described in Iqbal (1983). The following global atmospheric data sets are used to derive the clear-sky attenuation:

3.1. Rayleigh scattering and equally distributed gases

The Rayleigh scattering of the clear atmosphere and the absorption of equally distributed gas, mainly CO_2 and O_2 are taken into account using fixed values for the atmospheric components based on the U.S. Standard Atmosphere 1976. (U.S. Department of Commerce, 1976).

3.2. Ozone

Ozone absorbs radiation mainly at wavelengths smaller than 0.3 μm. Thus, the broadband attenuation

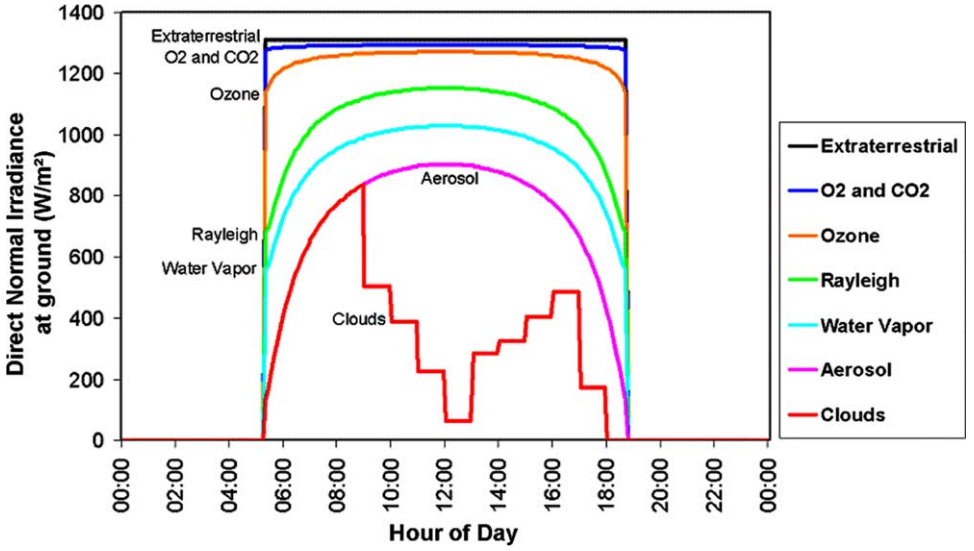

Fig. 1. Example of daily irradiance variation for true solar time showing the influence of the different atmospheric constituents on the direct normal irradiance. Values are calculated by the method presented here.

of DNI influenced by ozone is relatively small. The variability of stratospheric ozone mainly depends on the geographical latitude and the season. In the sunbelt regions the equivalent path length of ozone varies in the range from about 0.2 to about 0.4 cm at normal temperature and pressure (NTP) with moderate seasonal variability and a slightly decrease through the years. This affects the DNI on ground in the magnitude of lower ±1%. Therefore the use of zonal monthly mean values derived by the Total Ozone Mapping Spectrometer (TOMS onboard NASA's Earth Probe satellite) as input parameter is sufficient. The uncertainty of TOMS long-term mean values is quoted as 1% (McPeters et al., 1998). Data of TOMS are available for the period from 11/1978 until present.

3.3. Water vapour

Water vapour absorbs radiation mainly at thermal wavelengths. Its influence on the broadband attenuation of DNI is larger than that of ozone. Analysing monthly means of water vapour for four years for the sunbelt regions the mean spatial variability of the equivalent path length of water vapour for the investigated latitudes ranges from about 0.5 to about 6.5 cm[NTP] which results in a DNI-variability of ±15%. Due to this high variability we use mean daily values of precipitable water, that are based on 6-h values of the National Centers for Environmental Prediction (NCEP)—Reanalysis of the National Oceanic and Atmospheric Administration—Climate Diagnostic Center (CDC-NOAA). The spatial resolution is 2.5° × 2.5°. Daily data are available for the period from 01/1948 until present. More information about the NCEP-Reanalysis can be found in Kalnay et al. (1996). Fig. 2 gives an example of the data for North-Africa and the Mediterranean region.

3.4. Aerosol

Aerosols have a strong influence on the solar beam irradiance. Detailed information on aerosol optical thickness in a high temporal and spatial resolution is not yet available at a global scale. Such information would be useful because of the high spatial and temporal variability of aerosols. Depending on the region, AOT typically is in the range from 0.05 for clear coastal regions to greater than 2 for regions affected by desert dust during sand storms or soot during forest fires. This can decrease DNI close to 0 W/m^2, e.g. in a desert storm. A compromise between global availability and an appropriate spatial and temporal resolution was found in the climatological values of AOT derived by a transport model from the Global Aerosol Climatology Project (NASA-GACP) as shown in Fig. 3. This project was started 1998 within the NASA Radiation Sciences Program and the Global Energy and Water Cycle Experiment (GEWEX). GACP bases on the combination of global distributions of aerosol loading resulting from transport models for soil dust, sea salt, sulphate aerosols and carbonaceous aerosols. The used GACP model and the accuracy of the modelled aerosol optical thickness is described in Tegen et al. (1997), Chin et al. (2002) and Penner et al. (2002). More information on GACP can also be found in Mishchenko et al. (2002). The AOT of GACP is available for the wavelength of 550 nm. To use this AOT_{550} as input for the Bird model, which needs the AOT at the wavelength of 500 and 380 nm to calculate an effective broadband aerosol transmittance, following conversion is applied to the GACP data:

$$AOT_{500} = AOT_{550} \cdot \left(\frac{550}{500}\right)^{\alpha} \tag{3}$$

with the wavelength exponent α, which is set to 1.3, a typical value for different aerosol types, as suggested in Iqbal (1983). The same is done for AOT_{380} replacing the value 500 with 380.

Table 1 gives an overview of the spatial and temporal resolution for the above described clear-sky parameters, Table 2 describes the variability of the main clear-sky input parameters and their influence on the specific broadband transmittance based on the Bird model (airmass = 1). For example: looking at aerosol, high AOT

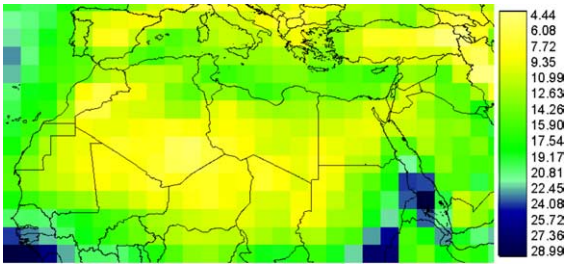

Fig. 2. Equivalent path length of water vapour (precipitable water, cm[NTP]), mean daily values for June 1998 for the North-African and Mediterranean region, according to NCAR-Reanalysis.

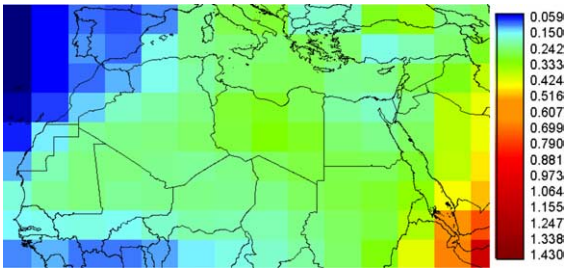

Fig. 3. Aerosol optical thickness of the wavelength 550 nm for June for the North-African and Mediterranean region, according to NASA-GACP.

Table 1
Overview of the used clear-sky parameters. Air-mass correction takes place in the model

Parameter	Spatial horizontal resolution	Temporal resolution	Available period
CO_2 and O_2	Constant	Constant	Constant
Rayleigh scattering	Constant	Constant	Constant
Ozone	5° zonal	Monthly mean	11/1978–present
Water vapour	2.5° lat × 2.5 °lon	Daily mean	01/1948–present
Aerosol (AOT)	4° lat × 5° lon	12 climatological monthly values	1 climatological year

Table 2
Overview of the variability of the main clear-sky input parameter and their influence on the specific broadband transmittance based on the Bird model (air-mass = 1)

Ozone		Water vapour		Aerosol	
cm[NTP]	τ_{Ozone}	cm[NTP]	τ_{WV}	AOT (550 nm)	$\tau_{Aerosol}$
0.2	0.990	0.5	0.921	0.05	0.934
0.3	0.985	1.5	0.895	0.20	0.806
0.4	0.982	2.0	0.888	0.40	0.674
		3.0	0.879	0.80	0.459
		4.0	0.870	1.00	0.368
		6.0	0.858	2.00	0.082

can decrease the DNI close to 0 W/m^2 (AOT = 2 → $\tau_{Aerosol} = 0.082$).

4. Cloud parameterisation

Solar irradiance at ground is mostly affected by clouds. In fact, beam irradiance can decrease close down to 0 W/m^2 due to clouds (as shown in Fig. 1), in contrast to global irradiance that is always substantially greater than 0 W/m^2 due to its diffuse fraction. Additionally, clouds have a high variability in space and time. Strong influence and high variability lead to a need of information on clouds in a high temporal and spatial resolution to meet the demand of accurate solar irradiance data at ground.

To use Bird's clear-sky model also for cloudy-sky conditions, DNI_{clear} is multiplied with an additional transmission coefficient for clouds, τ_{Cl}, based on a cloud detection algorithm developed by Mannstein et al. (1999). The bispectral cloud detection scheme uses infrared (IR) and visible (VIS) channels from the Meteosat-7 satellite. It is based on self adjusting, local thresholds which represent the surface conditions undisturbed by clouds. The calculated cloud-index (CI) is in the range of 0 for no clouds to 100 for completely cloudy pixels with high optical depth. CI represents the effective cloud transmission which is an integral value influenced by the cloud amount and by the average cloud optical depth within the analysed pixel. For each region within the Meteosat full disk shown in Fig. 4 the detection algorithm can be performed. Due to the spatial

Fig. 4. Example image of the Meteosat data used to derive the cloud index (Meteosat-7, coloured IR-Channel). © EUMETSAT, 2003.

range and the possible marginal position of the selected area of investigation within the Meteosat full-disk, the spatial resolution of the CI can range from 5 × 5 km^2 at the sub-satellite point to about 10 × 10 km^2 at marginal positions of the image.

In both spectral channels the basic principle of the algorithm is the same:

- Construct a reference image without clouds from previous images.

- Compare the actual image to the reference image to detect clouds.
- Update the information for the construction of the reference image using the cloud-free pixels.

Nevertheless there are differences in processing of both channels:

4.1. IR-scheme

The crucial task for getting a good estimate of cloud cover from an IR channel is the definition of a local temperature threshold as reference temperature which is close to the temperature of the cloud-free surface. As measurements of surface temperature are not available in a sufficient temporal and spatial resolution, we have to derive the reference temperature from the Meteosat data itself. To achieve this, we first calibrated the Meteosat count to obtain the equivalent black body temperature. We then sort the available images as a 3-dimensional array for each day with the spatial coordinates X and Y and the temporal coordinates T (time, every half hour, from 1 to 48). Single missing images do not affect this routine. The reference temperature of the land surface as shown in Fig. 5 is described by the following parametric function for every pixel:

$$T = a_0 + a_1(\cos(x - a_3 + \sin(a_2) \cdot \sin(x - a_3)) + 0.1 \cdot \sin(x - a_3)) \quad (4)$$

with $x = t/24 * 2\pi$ and $t =$ decimal hours of the satellite scan (UTC). a_0 gives the daily mean temperature, a_1 the temperature amplitude, a_2 influences the width and steepness of the daily temperature wave and a_3 gives the phase shift which is dominated by the local solar time. These four parameters are fitted daily for each land-pixel using the cloud-free pixels. Over sea only a_0 is variable, the other coefficients are set to zero (the temperature over sea is kept constant during one day).

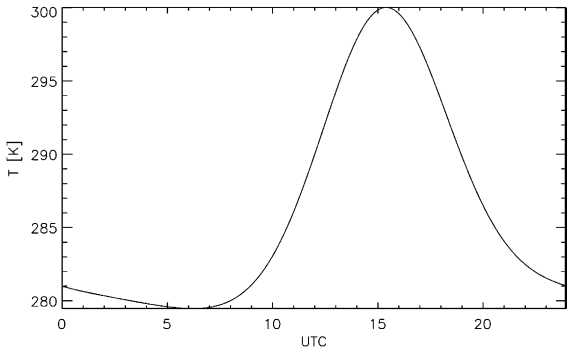

Fig. 5. Daily background temperature curve for a pixel over land surface derived from the fitting parameters $a_0 = 290.$, $a_1 = 10.$, $a_2 = 1.$ and $a_3 = 4.$ which are calculated by the IR-scheme.

The parameters are fitted from those pixels, which are with a high probability not contaminated by clouds and therefore representing the temperature of the land surface as it is measured by the satellite without any atmospheric correction. After the processing of 48 half-hourly images, we make an update on the coefficients a_0 to a_3. Both, new cloud-free temperature values and those derived from the coefficients enter into the new, weighted fit of the coefficients, which enables us to remember the surface properties even during longer cloudy periods. The weight of the old temperatures is reduced by 1/2 at each update, a fuzzy-logic combination of all cloud tests determines the weight of the new temperatures.

We use the following properties of surface vs. clouds for a first cloud detection:

- Clouds are cold. Every pixel with a temperature at least 4 K colder than the estimated reference temperature is valued as cloud. There is also an absolute temperature limit which depends on the region under consideration. For the sunbelt region we used −10 °C, a temperature which was not reached by the coldest surface pixels.
- Clouds move. We compare the data to the previous image and the image of the day before. Clouds are colder and show up as local differences.
- Surface temperature has a regular daily variation and depends on the landscape. We compare the data to the predicted reference image. Clouds again show up as local differences.
- Weather patterns have a larger scale than pixel size. We allow for deviations from the predicted reference temperatures if they are of the same magnitude within regions of pixels with similar surface properties. This information is used to make an additive update of the predicted surface temperature.

As the quality of the predicted reference data is variable, the decision process depends on weights similar to a fuzzy-logic decision. Fig. 6 shows the IR-cloud detection scheme for North-Africa and the Mediterranean Sea for the date of June 21st 1998, 11:00 UTC. The actual IR-image is shown in Fig. 6(a) with the measured temperature in °C. The mean temperature a_0 is given in Fig. 6(b); Fig. 6(c) shows the temperature amplitude a_1 which is constant zero for the sea and therefore consistent black. Over land a_1 varies depending on the surface properties: the brighter the pixel the higher the difference between day and night temperature. The cloud-free reference temperature for 11:00 UTC is shown in Fig. 6(d). The result is presented in Fig. 6(e) where the surface features vanished nearly completely. The long-lasting cloudiness in the southern part did not allow for a satisfying determination of the coefficients for the

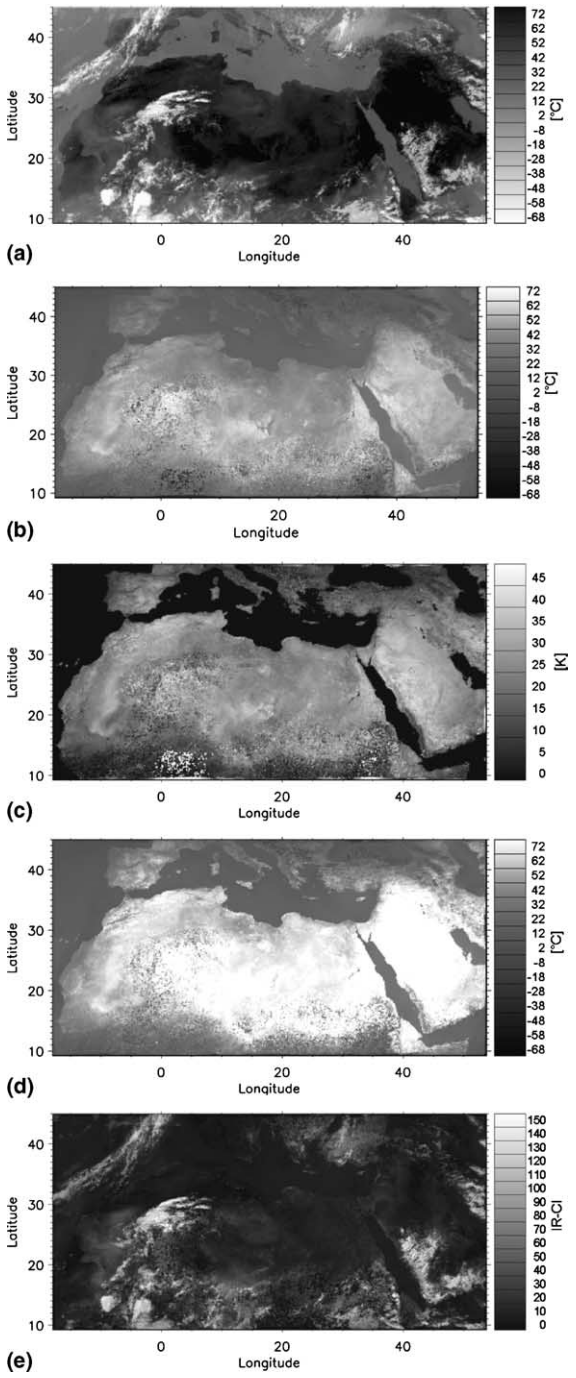

Fig. 6. (a) Actual Meteosat IR data; (b) Coefficient a_0 (mean temperature value); (c) Coefficient a_1 (temperature amplitude); (d) Calculated cloud-free image; (e) Difference between calculated cloud-free image (d) and actual Meteosat data (a). All figures refer to the date of June 21st 1998, 11:00 UTC.

reference temperature. Nevertheless clouds are detected there by this method.

4.2. VIS-scheme

Different from the infrared data, the daily variation of the reflected sunlight data is mainly influenced by geometrical factors. The uncalibrated Meteosat counts are first corrected against the local solar zenith angle. For further corrections we analyse one year of full disk VIS data. From several combinations of two angles we select the distribution of corrected counts with respect to the solar zenith angle and the angular distance of Meteosat to the specular reflection direction in a 3-D histogram as shown in Fig. 7. This combination of angles was motivated by the correction of sunlight over water surfaces, but seems to explain the daily variation of the apparent surface reflectance sufficiently. We selected the 1% percentile to represent the minimum count which is subtracted from the data to account for atmospheric influences like forward and backward scattering within the atmosphere. VIS data is included into the decision process at locations, where the sun elevation angle is greater than 5.7°. The VIS information is weighted proportional to the cosine of the solar zenith angle, as the uncertainties increase with low solar elevation. Similar to the IR, we derive from the data a reference image, which is in this case not variable throughout the day. The actual VIS images are compared against the predicted reference image and the previous image. The corrected count has to be higher than a threshold derived from the predicted 'cloud-free' scene. Fig. 8(a) shows the actual VIS-image, the reference image Fig. 8(b) and the resulting image Fig. 8(c) again for North-Africa and

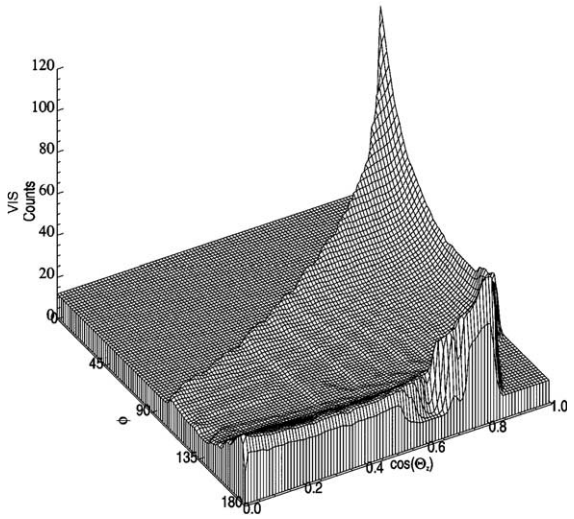

Fig. 7. Meteosat minimum VIS-counts depending on the cosine of solar zenith angle Θ_Z and the angular distance ϕ between solar specular reflectance and satellite as seen from surface.

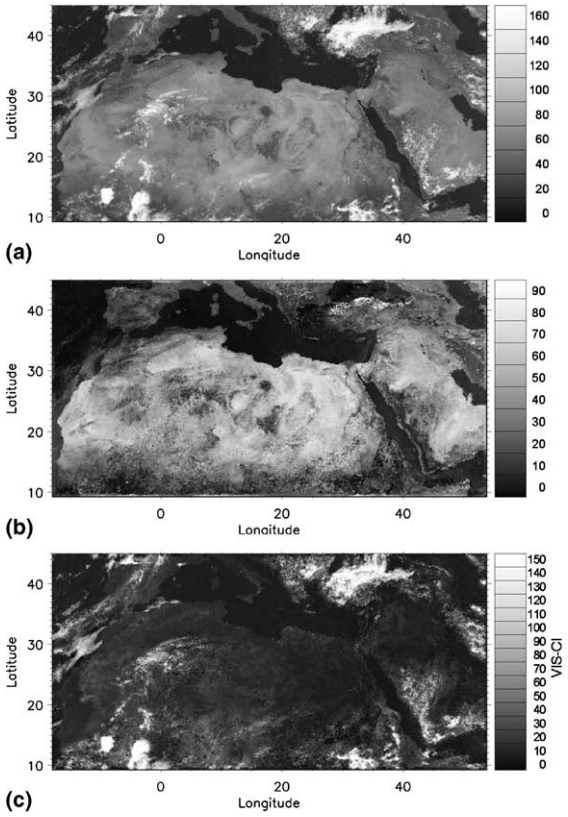

Fig. 8. (a) Actual Meteosat VIS data; (b) calculated reference image (c) difference between calculated cloud-free reference image (b) and actual Meteosat data (a). All figures refer to the date of June 21st 1998, 11:00 UTC.

the Mediterranean Sea for the date of June 21st 1998, 11:00 UTC.

Both, IR and VIS information are combined to select those values that are used for the update of the clear-sky properties and also for the final calculation for the cloud-index CI. The self-learning cloud-algorithm needs several days lead time to calculate the reference fit. Fig. 9(a) shows the 2-dimensional histogram for the used VIS and IR channel. The position of the values within the histogram can be used for a classification. Snow and ice can not be detected using this method.

4.3. Cloud index

From the IR and VIS channels, a cloud index is derived by linear interpolation between the expected 'cloud-free value' and a threshold for a 'fully cloudy' pixel. From empirics we have chosen −40 °C in the IR and a corrected count of 150 in the VIS channel. The 2-dimensional histogram in Fig. 9(b) shows the difference value in the IR and VIS. The cloud-free values are now close to [0,0], strong positive deviations in both directions are indicators for cloudiness. The CI is chosen as the maximum of IR and VIS cloud index and then limited to the range 0–100 (Fig. 10).

To simulate hourly mean values a simple filter is selected which weights the scenes before and after the nominal time with 25%, while the scene at nominal time is weighted with 50%. For example, the cloud index value for the 12th hour of the day is the weighted mean value from the indices derived from the nominal times at 11:00, 11:30 and 12:00 as described in Eq. (4).

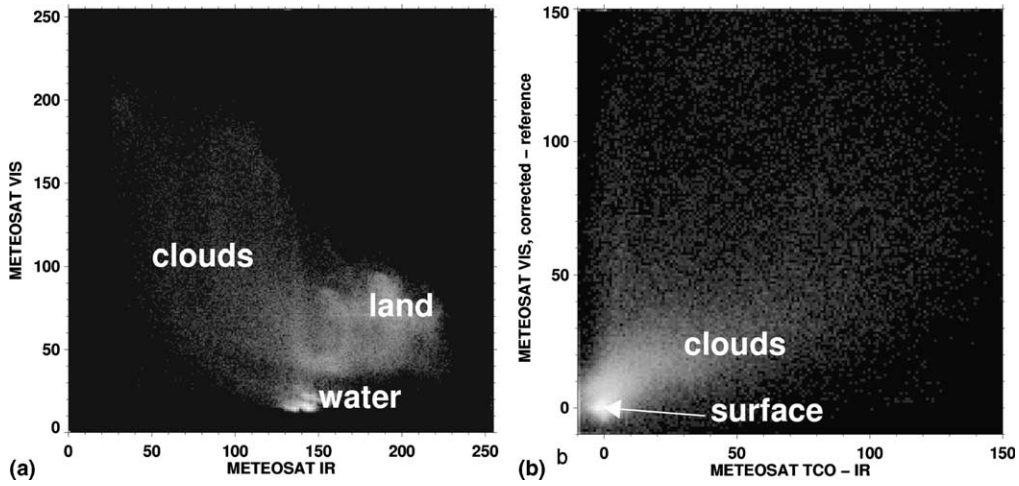

Fig. 9. (a) 2-D Histograms of IR (Fig. 6 a) vs. VIS (Fig. 8 a); (b) differences to the calculated surface values in Figs. 6e and 8c on the right. Clear-sky pixel cluster here at the [0,0] point, while deviations in both directions, i.e. colder and brighter, have to be considered as cloud contaminated. All figures refer to the date of June 21st 1998, 11:00UTC.

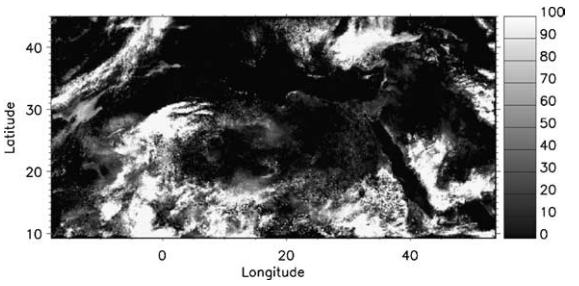

Fig. 10. Cloud index derived for North-Africa and the Mediterranean region for June 21 1998, 11:00 UTC.

$$CI_{nom12:00} = 0.25 \cdot CI_{11:00} + 0.5 \cdot CI_{11:30} + 0.25 \cdot CI_{12:00} \quad (5)$$

Conversion of the resulting CI into an effective cloud transmissivity τ_{CI} is done by

$$\tau_{CI} = \frac{100 - CI}{-100} \quad (6)$$

According to the validations in Schillings et al. (2004) this simple linear relationship proofed to be a good approximation for effective cloud transmissivity related to Meteosat pixels. It should be noted that this good agreement is achieved without any statistical adaptation to ground measurements of the DNI.

Using the above described DNI and CI calculation scheme following shortcomings and strengths should be considered: The used clear-sky parameterisation model results in a reduced accuracy due to the broadband calculation scheme but achieved a fast calculation process. As the cloud detection scheme extracts information for defining the reference image out of the Meteosat data itself, longer cloudy periods (up to 3–4 weeks) complicate the definition of a reliable reference image for the VIS and in the IR data. The scheme improves the detection of cloud cover for low sun elevation angles and of thin cirrus due to the additional use of Meteosat IR-data. The daily variability of aerosol can not be reproduced by the used monthly climatological aerosol optical thickness, but the global availability of all atmospheric input data and the detection of cloud cover information and calculation of the DNI independent from ground measurements offer the possibility for a world wide solar energy resource assessment using geostationary satellite data.

5. Conclusion

We described a fast parameterised model to calculate hourly solar direct normal irradiance DNI. As clouds have the strongest impact on beam irradiance at ground, the resolution of the cloud parameterisation dominates the overall spatial (nominal 5 km × 5 km) and temporal (hourly) resolution. The main feature of the presented method is the use of Meteosat IR-data for cloud detection and the definition of a reference temperature curve for each pixel and each day. The difference between the reference and the actual image is interpreted as cloud index. Meteosat VIS-data help for the detection of low clouds which cannot be detected in the infrared.

It should be possible to adapt the presented cloud cover algorithm for all other geostationary satellites equipped with infrared and visible channels. As auxiliary data of ozone (NASA-TOMS), water vapour (NCEP-NCAR), aerosol (NASA-GACP) and elevation (DEM-GLOBE) used for the DNI-scheme are available globally the method may also be applied world-wide. Such a global solar energy assessment is performed for example through the UNEP-project SWERA (UNEP, 2001). The calculated DNI can be used as high-quality input parameter for simulation and planning of concentrating solar systems, e.g. parabolic trough, power tower technology or dish stirling systems. Planning tools like greenius (Quaschning et al., 2001), RETScreen (Leng et al., 1998) or STEPS (Broesamle et al., 2001; Kronshage et al., 2002) are already available and can find a wide application if reliable irradiance data is easily available.

Using data of the new Meteosat, called Meteosat Second Generation (MSG) can lead to a higher temporal (15 min) and higher spatial (up to 1.25 × 1.25 km^2) resolution for the cloud cover. Cloud detection and classification can be improved by using additional available channels onboard MSG. We plan to use more detailed aerosol data derived by new satellites (ENVISAT, MODIS etc.) in the future.

Acknowledgements

All Meteosat data is under copyright of EUMETSAT, Darmstadt, Germany. Many thanks for access to the data set go to the crew of the MARF (Meteosat Archive and Retrieval Facility, Darmstadt) and to our colleagues from DLR-DFD (Deutsches Fernerkundungs-Datenzentrum).

Data on aerosol is provided by NASA-GACP Global Aerosol Climatology Project.

We also acknowledge the use of the water vapour data from the NCEP Reanalysis by NOAA-CIRES Climate Diagnostics Center, Boulder, Colorado, US and the use of the TOMS ozone data provided by the NASA-Goddard Space Flight Center (GSFC), Washington, DC, USA.

Special thanks to Dr. Franz Trieb at DLR-Stuttgart for his comments and helpful discussions.

References

Battles, J.F., Olmo, F.J., Tovar, J., Alados-Arboledas, L., 2000. Comparison of cloudless sky parameterisation of solar irradiance at various spanish midlatitude locations. Theo. Appl. Climatol. 66, 81–93.

Bird, R.E., Hulstrom, R.L., 1981. Review, evaluation and improvement of direct irradiance models. J. Sol. Energy Eng. 103, 182–192.

Broesamle, H., Mannstein, H., Schillings, C., Trieb, F., 2001. Assessment of solar electricity potentials in North Africa based on satellite data and a geographic information system. Sol. Energy 70 (1).

Cano, D. et al., 1986. A method for the determination of the global solar radiation from meteorological satellite data. Sol. Energy 37 (1), 31–39.

Chin, M. et al., 2002. Tropospheric aerosol optical thickness from GOCART model and comparison with satellite and sunphotometer measurements. J. Atmos. Sci. 59 (3), 431–483 (Special Issue of Global Aerosol Climate).

EUMETSAT, 2003. Overview of Meteosat calibration (http://www.eumetsat.de/en/index.html?area=left7.html&body=/en/dps/mpef/calibration.html&a=730&b=1&c=700&d=700&e=0).

Fröhlich, C., Brusa, R.W., 1981. Solar radiation and its variation in time. Sol. Phys. 74, 209–251.

Gautier, C.M., Diak, G., Masse, S., 1980. A simple physical model to estimate incident solar radiation at the surface from GOES satellite data. J. Appl. Meteorol. 19, 1005–1012.

Gueymard, C., 1993. Critical analysis and performance assessment of clear-sky solar irradiance models using theoretical and measured data. Sol. Energy 51 (2), 121–138.

Hammer, A., Heinemann, D., Hoyer, C., Kuhlemann, R., Lorenz, E., Mueller, R., Beyer, H.G., 2003. Solar energy assessment using remote sensing technologies. Remote Sens. Environ. 86 (3), 423–432.

Hastings, D.A., Dunbar, P.K., 1998. Development & assessment of the global land one-km base elevation digital elevation model (GLOBE). Int. Soc. Photogramm. Remote Sens. (ISPRS) Arch. 32 (4), 218–221. (http://www.ngdc.noaa.gov/seg/topo/globe.shtml).

Ineichen, P., Perez, R., 1999. Derivation of cloud index from geostationary satellites and application to the production of solar irradiance and daylight illuminance data. Theor. Appl. Climatol. 64, 119–130.

Iqbal, M., 1983. An Introduction to Solar Radiation. Academic Press, Toronto.

Kalnay, E. et al., 1996. The NMC/NCAR 40-year reanalysis project. Bull. Am. Meteorol. Soc. 77 (3), 437–472.

Kronshage, S., Schillings, C., Trieb, F., 2002. Country analysis for solar-thermal power stations using remote sensing methods. In: Proc. of World Renewable Energy Congress VII, Cologne, Germany. (http://www.dlr.de/steps).

Leng, G., et al., 1998. RETScreenTM—renewable energy technologies project assessment tool—version 98, report # EDRL 98-05 (TR), CANMET Energy Diversification Research Laboratory, Natural Resources Canada, Varennes, April 1998, p.332. (http://retscreen.gc.ca).

Mannstein, H., Broesamle, H., Schillings, C., Trieb, F., 1999. Using a Meteosat cloud index to model the performance of solar-thermal power stations. In: Proceedings of EUMETSAT Conference, Copenhagen, pp. 239–246.

Mayer, B., 1999. I3RC phase 1 results from the MYSTIC Monte Carlo model. In: Proceedings of the I3RC workshop, Tucson, Arizona.

McPeters, R.D., et al., 1998. Earth Probe Total Ozone Mapping Spectrometer (TOMS) Data Products User's Guide. NASA Technical Publication 1998-206895.

Mishchenko, M., Penner, J.E., Anderson, D. (Eds.), 2002. Global Aerosol Climatology Project J. Atmos. Sci. 59 (3), Special Issue of Global Aerosol Climate.

Möser, W., Raschke, E., 1983. Mapping of global radiation and of cloudiness from Meteosat data. Meterol. Rundschau 36, 33–41.

Penner, J.E. et al., 2002. A comparison of model- and satellite-derived aerosol optical depth and reflectivity. J. Atmos. Sci. 59 (3), 441–460, Special Issue of Global Aerosol Climate.

Perez, R. et al., 2002. A new operational satellite-to-irradiance model—description and validation. Solar Energy 73 (5), 307–317.

Pinker, R.T., Ewing, J.A., 1985. Modelling surface solar radiation: model formulation and validation. J. Appl. Meteorol. 24, 389–401.

Quaschning, V., Ortmanns, W., Kistner, R., Geyer, M., 2001. Greenius—a new simulation environment for technical and economical analysis of renewable independent power projects. In: ASME International Solar Energy Conference Solar Forum 2001. Washington DC, 22–25. April 2001, pp. 413–417. (http://www.greenius.net/en/start.html).

Rigollier, C., Lefèvre, M., Wald, L., 2001. Heliosat version 2. EU-project SODA: integration and exploitation of networked solar irradiation databases for environment monitoring. Deliverable No. D3.2. IST-1999-12245.

Schillings, C., Meyer, R., Mannstein, H., 2004. Validation of a method for deriving high resolution direct normal irradiance from satellite data and application for the Arabian peninsula. Solar Energy (this volume), doi:10.1016/j.solener.2003.07.037.

Stuhlmann, R., Rieland, M., Raschke, E., 1989. An improvement of the IGMK model to derive total and diffuse solar radiation at the surface from satellite data. J. Appl. Meterol. 29, 586–603.

Tarpley, J.D., 1979. Estimating incident solar radiation at the surface from geostationary satellite data. J. Appl. Meteorol. 18, 1172–1181.

Tegen, I., Hollrig, P., Chin, M., Fung, I., Jacob, D., Penner, J.E., 1997. Contribution of different aerosol species to the global aerosol extinction optical thickness: estimates from model results. J. Geophys. Res. 102, 23895–23915.

UNEP, 2001. SWERA—Solar and Wind Energy Resource Assessment (http://swera.unep.net).

U.S. Department of Commerce, 1976. U.S. Standard Atmosphere, 1976, U.S. Government Printing Office, Washington, D.C., 1976.

Wyser, K. et al., 2002. Remote sensing of surface solar irradiance with corrections for 3-D cloud effects. Remote Sens. Environ. 80, 272–284.

Zelenka, A., Perez, R., Seals, R., Renné, D., 1999. Effective accuracy of satellite-derived irradiance. Theor. Appl. Climatol. 62, 199–207.